Definition of critical hydrodynamic conditions for sediment motion initiation using optical techniques.

JUAN ANTONIO GARCÍA ARAGÓN, KLEVER IZQUIERDO AYALA, HUMBERTO SALINAS TAPIA and CARLOS DÍAZ DELGADO.
Centro Interamericano de Recursos del Agua, Facultad de Ingeniería.
Universidad Autónoma del Estado de México.
Cerro de Coatepec, CU, 50130, Toluca, Edomex
MEXICO
jagarciaa@uaemex.mx http://www.uaemex.mx/cira

Abstract: Sediment motion initiation experiments were performed in a glass rectangular channel, with a loose bed in the central part. The main goal is to obtain the critical hydrodynamic characteristics that causes sediment bed motion initiation, for different cohesionless sediment grain sizes. The optical technique of Particle Tracking Velocimetry (PTV) was used in order to determine the critical velocity profiles for sediment initiation of motion. Between the parameters that define this critical velocity profile is the one known as bed rugosity which represents the height of asperities in the bed. For conditions near bed motion initiation experimental velocity profiles were obtained and they allowed us also to define fluctuating velocities u´, v´ and a value of bed rugosity *ks* related to a representative grain size of the bed. It was shown that obtained critical velocity profiles are in good agreement with other works in the scientific literature provided an appropriate definition of bed rugosity is made.

Key-Words: non-cohesive sediments, motion initiation, bed rugosity, critical velocity profile, PTV.

1. Introduction

In order to define the critical conditions for bed motion initiation in beds formed by cohesionless sediments a lot of work has been done [1]. The most known work is that of Shields [2] who, based on experimental data for bed motion initiation, related the bed shear stress to a dimensionless parameter. Yalin and Karahan [3] extended the findings to laminar flow. Later work for motion initiation has shown that the magnitude of critical shear stresses differs slightly from that of Shields but the shape of the curve is preserved ([4], [5], [1], [6], [7], [8], [9]). Research has been focused on the bed packing and sizes non-uniformities in order to obtain statistical parameters that relate in a better way the critical bed shear stress to a particle size parameter ([10], [11], [12]). River beds are constituted by a sediment mixture of different sizes and common engineering practice has been to extrapolate experimental data results with uniform size sediments to non-uniform sediment beds ([13], [14], [15]).

The critical velocity profile is defined as the one that causes motion initiation. In order to define it, bed rugosity should be chosen appropriately, it is a parameter that represents the height of roughness of the bed. Nikuradse (cited by [1]) proposes for bed rugosity the mean diameter of the bed. In the case of non-uniform bed the largest diameters are intuitively more appropriate to represent bed rugosity. In the scientific literature it is common to represent bed rugosity as the mean diameter or another representative diameter multiplied by a factor larger than one. The problem is then to choose an appropriate representative diameter and an appropriate factor ([1], [16]).

The best representation of the interaction between the bed and the flow is the velocity profile. It has been shown that the best representation of the velocity profile is a logarithmic approximation, which includes a parameter named bed rugosity. Shear stress is implicitly represented in the velocity profile [16]. The critical velocity profile for bed motion initiation is defined as the velocity profile obtained when the critical shear stress is actuating. In this work this critical velocity profile was measured using the optical technique Particle Tracking Velocimetry (PTV) [17]. Five different combinations of shear stresses-critical velocity profile were obtained and bed rugosity was deduced for these five different sizes of sand at bed motion initiation.

Optical techniques like PTV are useful to measure turbulence and Reynolds stress distribution. This is a way to obtain the shear stress, also for difficult situations like in rivers where friction slope is not obtained straightforward. In this work shear velocity and shear stress were obtained using the fluctuating velocities measured for each velocity profile ([18], [19]).

Paragraph 2 presents a summary of the main work done to represent critical conditions for sediment motion initiation and the approach taken in this work to define the critical velocity profile. Paragraph 3 presents the optical technique used in this work Particle Tracking Velocimetry (PTV), the experimental set-up and the characteristics of the beds used. In paragraph 4 the equations used to calculate bed rugosity are presented and in paragraph 5 experimental results are presented and compared with other formulas in the scientific literature.

2. Problem Formulation

The known Shields diagram [2] is the graphical representation of the critical condition for motion initiation. It relates two dimensionless parameters, the Shields parameter Θ and the particle Reynolds Re_p

$$\theta = \frac{\tau_c}{D(\gamma_s - \gamma)} \qquad (1)$$

$$\mathrm{Re}_p = \frac{u_* D}{\nu} \qquad (2)$$

where τ_c = critical shear stress (N/m^2); D = mean diameter of bed particles (m); γ_s = specific weight of particles (N/m^3); Y = specific weight of the fluid (N/m^3), ν = kinematic viscosity of the fluid (m^2/s) and u_* = shear velocity (m/s), $u_* = (\tau/\rho)^{1/2}$, where ρ = fluid density (kg/m^3).

Using those parameters and the logarithmic velocity profile, Chien and Wan [1] propose the following equation

$$\frac{U_c}{\sqrt{\frac{\gamma_s - \gamma}{\gamma} gD}} = 5.75\sqrt{f(R_{ep})}\log 12.27\frac{\chi R}{k_s} \qquad (3)$$

where U_c = mean critical velocity for motion initiation (m/s), R = hydraulic radius (m), k_s = bed rugosity (m), g = gravity acceleration (m^2/s), X = constant and $f(Rep)$ is a function of Re_p or Shields parameter Θ for bed motion initiation. Considering Shields(1936) results for Re_p larger than 60 the value of Θ is close to 0.045, and equation 3 becomes

$$\frac{U_c}{\sqrt{\frac{\gamma s - \gamma}{\gamma} gD}} = 1.219\log 12.27\frac{\chi R}{k_s} \qquad (4)$$

Einstein [20] define χ as a function of the relationship k_s/∂, for rough bed $k_s/\partial > 10$, $\chi = 1$, if $k_s/\partial < 0.25$ then we have smooth bed $\chi = 0.3u_* k_s/\nu$; the maximum $\chi = 1.6$ is obtained in the transition zone for $k_s/\partial = 1.0$; ∂ is the depth of the viscous sublayer. Some formulas in the scientific literature have the form of equation 4. Between them the equation of Goncharov

$$\frac{U_c}{\sqrt{\frac{\gamma_s-\gamma}{\gamma}gD}} = 1.06\log\frac{8.8h}{D_{95}} \quad (5)$$

where h = flow depth. And the equation of Levy [22]

$$\frac{U_c}{\sqrt{gD}} = 1.4\log\frac{12R}{D_{90}} \quad (6)$$

The main difference between these formulations is the definition of bed rugosity k_s. For these authors bed rugosity is represented by the largest bed diameter D_{95} or D_{90} respectively ([1] , [6]). Others magnitudes of bed rugosity has been proposed, Ackers and White [1] define k_s = 1.25 D_{35}, Engelund and Hansen [1] propose k_s = 2 D_{65}, Einstein [20] suggest $k_s = D_{65}$. Van Rijn [23] made a review of different authors and conclude that the rugosity of a flat bed and loose varies from 1 to 10D_{90} recommending as mean rugosity to be used k_s = 3 D_{90}. It can be concluded that bed rugosity is defined in the literature as the representative diameter multiplied by a constant larger than one. Engelund and Bayazint (cited by [24]) propose that the representative diameter is that where settling velocity is equal to the mean settling velocity of the mixture of particles. The logaritmic law of velocity distribution [16] can be expressed as

$$\frac{u}{u_*} = \frac{1}{k}\ln\frac{y}{k_s} + B \quad (7)$$

The constant B included in this logaríthmic velocity distribution has been obtained experimentally using the hydraulic boundary condition. Fuentes and Carrasquel (cited by [16]) propose the following approximation to obtain B as a function of Reynolds of the rugosity R_*.

$$B = -\frac{1}{k}\ln\left[\frac{1}{9.025R_*} + \frac{1}{30}e^{\left(-10.78/R_*\right)}\right] \quad (8)$$

where k = Von Karman constant, in this case $k = 0.4$ (low solids concentration) [25]. The parameter R_* (Reynolds of the rugosity) is expressed in function of bed rugosity ks

$$R_* = \frac{u_* k_s}{\nu} \quad (9)$$

The Reynolds stress is the term that considers the total shear stress distribution

$$\tau = -\rho\overline{u'v'} = \rho u_*^2\left(1 - y/h\right) \quad (10)$$

where y = height above bed; u'= fluctuating velocity in flow direction and v' = vertical fluctuating velocity. This flow distribution has been validated for turbulent open channel flow by [19]. They compare the shear stress based on friction slope S with the one obtained by measuring the Reynolds stress profiles ([26], [27]) . The optical technique PTV used in this work allow us to measure velocity fluctuations hence the Reynolds stresses and obtain a value of shear velocity u_* ([28], [29], [30]).

3. Experimental measurements

3.1 Particle Tracking Velocimetry

Experimental optical techniques are suitable for measuring flow characteristics at motion initiation because it does not disturb the flow. In this work the optical technique of Particle Tracking Velocimetry (PTV) was used. An algorithm to make more efficiently the pairing of particles was developed.

It is known that the image intensity of a particle is obtained by the square of the convolution from the response function to lens impulse and the geometric image of the particle. This condition is valid when the flow is seed by spherical uniform particles.

However for some issues where the seed particles in the flow are non-spherical and non-uniform, as the case of sediment transport specific algorithms should be developed. This is why we worked the algorithm presented in this paper.

The algorithm has six steps:

a) Maximum intensity identification for some particle sizes.

b) Obtaining particle shape.

c) Particle image centroid finding.

d) Particle pairs identification

e) Particle velocity calculation.

f) Beginning new process for another particle size.

The first step of the algorithm finds the maximum intensity of the particles images for a given size in the flow field. Then the first search of particle image intensities is given by the following condition:

$$I^1_{\min} \le I^1 \le I^1_{\max} \tag{11}$$

where I^1 are intensities for larger size particles and $[I^1_{\min}, I^1_{\max}]$ are search limits. Once the maximum intensities are identified for a given particle size, the particle shape is obtained. From the maximum intensity píxel a radial search is performed to find the particle shape according to the following condition

$$I^1_p < I^1 \tag{12}$$

where I^1_p is a lower intensity than I^1 and belonging to a given particle size.

The next step is to find the centroid of the particle image shape. Considering the particle intensity distribution of an image I^1_p in each pixel coordinate (x_i, y_i), the intensity value is $I^1_p(x_i, y_i)$. The algorithm finds the centroid (x_c, y_c) from the points group $\{(x_i, y_i)\}$ weighting each point by the intensity value, this is

$$(x_c, y_c) = \frac{\sum_i \sum_j (x_i, y_j) I^1_p(x_i, y_j)}{\sum_i \sum_j I^1_p(x_i, y_j)} \tag{13}$$

The centroid is usually known as first order moment. The calculation requires to identify the particle and to limit the area over which the calculation is performed. The centroid is obtained for each particle.

For particle pairing the first step is to identify a particle in the first laser pulse, then the particle centroid is found in the second pulse.

$$d_{\min} \le \left| \bar{x}_i - \bar{x}_j \right| \le d_{\max} \tag{14}$$

where $\bar{x}_i, \bar{x}_j$ are the coordinates of the particles centroid in the first and second pulse, d_{min} and d_{max} are minimum and maximum distances to the centroid of the first particle. This distance defines the right pair and depends on the particle size and a pre-estimated velocity. However because the particle does not follow the flow direction, it is also compulsory to take into account the particle direction, $\theta_{\min} \le \theta \le \theta_{\max}$ where $\theta_{\min}, \theta_{\max}$ are the limits of the particle directions, usually $\theta_{\min}$ is considered zero (figure 1).

After choosing pairs, centroids are defined and eliminated for the next pair detection. Then the distance between particles is obtained. If we want to obtain particles of the same characteristics the limits are compulsory

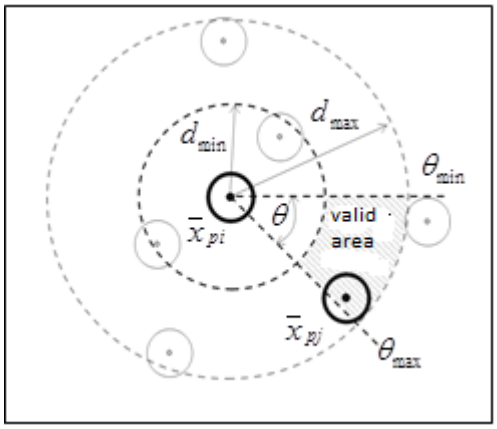

Fig. 1 Representation of the conditions to obtain particle pairs.

The final step after pair identification and distance calculation between particles is the definition of the components of the velocity vector *(u,v)* for each pair. This is done with the distance between particles d(x) in the horizontal and d(y) in the vertical and time of image capture *(Δt)*

$$(u.v) = \left(\frac{d(x)}{\Delta t}, \frac{d(y)}{\Delta t} \right) \tag{15}$$

the result is obtained in px/seg, an equivalent factor (magnification) relating cm/px is needed, in order to obtain the components in cm/seg.

Process continue for another particle size according to the following condition

$$I^2_{min} \le I^2 \le I^2_{max}, \text{ where, } I^1_{\min} < I^2_{\max} \tag{16}$$

and works for different sizes as follows

$$I^n_{min} \le I^n \le I^n_{max}, \text{ and, } I^{n-1}_{min} < I^n_{max} \tag{17}$$

For each particle size steps b, c, d and e are repeated.

3..2 Sand Characteristics

Sand from a quartz mine was used to obtain the five (beds) with different *D*. The density and specific weight are ρ_s = *2 543 Kg/m*^{3} and γ_s = *24 950 N/m*^{3}. Table 1 presents sand characteristics. An average value *D* is also presented. The American Geophysical Union classification for each bed is also presented.

The experiments for motion initiation were developed in a 220 cm long channel with a width of 10 cm. The sand was colocated in a trench in the middle of the channel with a flat configuration at the start. Figure 2 shows the experimental set up with the accesories used in the optical technique PTV. Polyamide particles of 5 μm were used as tracers. A 4 W ion-argon laser was used and a chopper to pulse the laser light. CCD cameras were synchronized with laser pulses in order to obatin images in succesive laser pulses. Image analysis was done with a software developed for this research SEDPTV. The analysis region for PTV was the center of the channel parallel to flow direction

Table 1 . Bed characteristics

Loose bed	**Maximun Size D_{mx}(mm)**	**Minimun Size D_{mn}(mm)**	**Average Size D (mm)**	**AGU Classification**
S1	0.425	0.333	0.379	Medium sand
S2	0.850	0.425	0.638	Coarse sand
S3	1.000	0.850	0.925	Coarse sand
S4	2.360	1.000	1.680	Very coarse sand
S5	4.000	2.360	3.180	Very fine gravel

.

The velocity profiles obtained comes from an average 7000 data of velocity in flow direction, u and the vertical direction, v, at different depths of flow *y* until *h*. A cross correlation allowed us to obtain the best fit curve of the form

$$y = Ae^{b_0 u} \tag{18}$$

Where, *y* = depth over the bed (m), *u* = velocity in the flow direction (m/s), and *A*, b_0 regression constants.

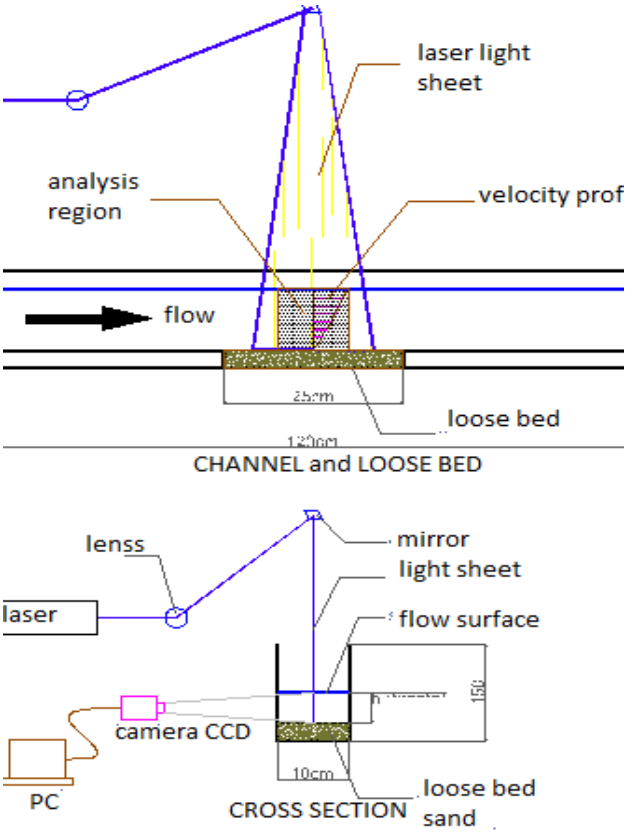

Fig. 2 Image capture and processing in a flow region over loose bed

Motion initiation was simulated by increasing the flow rate until a visual evident motion of sediment was obtained. Velocity profiles were obtained for flow rates previous to motion initiation and for motion initiation. Shear velocity was calculated taking into account the Reynolds shear stresses, according to the following equation

$$u_* = (\overline{u'v'})^{1/2} = \sqrt{\frac{1}{N}\sum_{N}^{i=1}(u_i - U_x)(v_i - V_m)} \tag{19}$$

Where U_x = Mean velocity in the flow direction; V_m = mean flow velocity in the vertical direction; *u'* and *v'* are the fluctuating velocities *in x and y* ; and N =total velocity data used to perform the regression. The mean velocities U_x and V_m are obtained in the following way

$$U_x = \left\lfloor \frac{h}{b_0}\ln\left(\frac{h}{A}\right) - \frac{h}{b_0}\right\rfloor + \left\lfloor \frac{A}{b_0}\right\rfloor \tag{20}$$

$$V_m = \frac{1}{N}\sum_{N}^{i=1} v_i \tag{21}$$

4. Bed rugosity determination

From the regression curve of the experimental data and from logarithmic velocity profile equations 22 and 23 are obtained

$$\ln(y) = \ln(A) + b_0 u \tag{22}$$

$$\ln(y) = \frac{k}{u_*}u + \ln(k_s) - Bk \tag{23}$$

Then, the following relationship is obtained from those equations

$$\ln(A) = \ln(k_s) - Bk \tag{24}$$

Equation 24 contains two unknowns k_s and the constant *B*. Using an expression for *B* proposed by Fuentes-Carrasquel [16] is written as

$$\ln\left(\frac{k_s}{A}\right) = -\ln\left\lfloor \frac{1}{9.025(R_*)} + \frac{1}{30}e^{\left(-10.78/(R_*)\right)}\right\rfloor \tag{25}$$

Bed rugosity k_s is obtained by solving equation 25 for the experimental data. It should be taken into account that R_* depends on u_* which can be calculated with the shear stresses obtained with the fluctuating velocities equation 19.

5. Results

Figure 3 shows the data obtained for each sand bed at different runs whit the same flow rate and the corresponding average velocity profile from correlation analysis.

Simulations of motion initiation were developed for each of the five sand grains. In each simulation an average of 10 velocity profiles were obtained before motion initiation. The maximum velocities applied to the bed *S5 = 3.180mm* were not enough to obtain motion initiation. Table 2 presents mean velocities and shear stresses for the motion initiation of the five beds analized. It includes also the conditions used to start the simulations (minimum flow conditions).

Table 2. Shear stresses and velocities for motion initiation

Loose bed	Average size *D(mm)*	minimum		motion initiation	
		τ_0 (N/m^2)	U_x (cm/s)	τ_c (N/m^2)	U_c (cm/s)
S1	0.379	0.196	19.544	0.315	25.809
S2	0.638	0.252	21.764	0.438	27.912
S3	0.925	0.247	23.379	0.554	31.848
S4	1.680	0.412	29.648	0.953	38.202
S5	3.180	0.429	29.315	maximum (no motion)	
				2.253	70.252

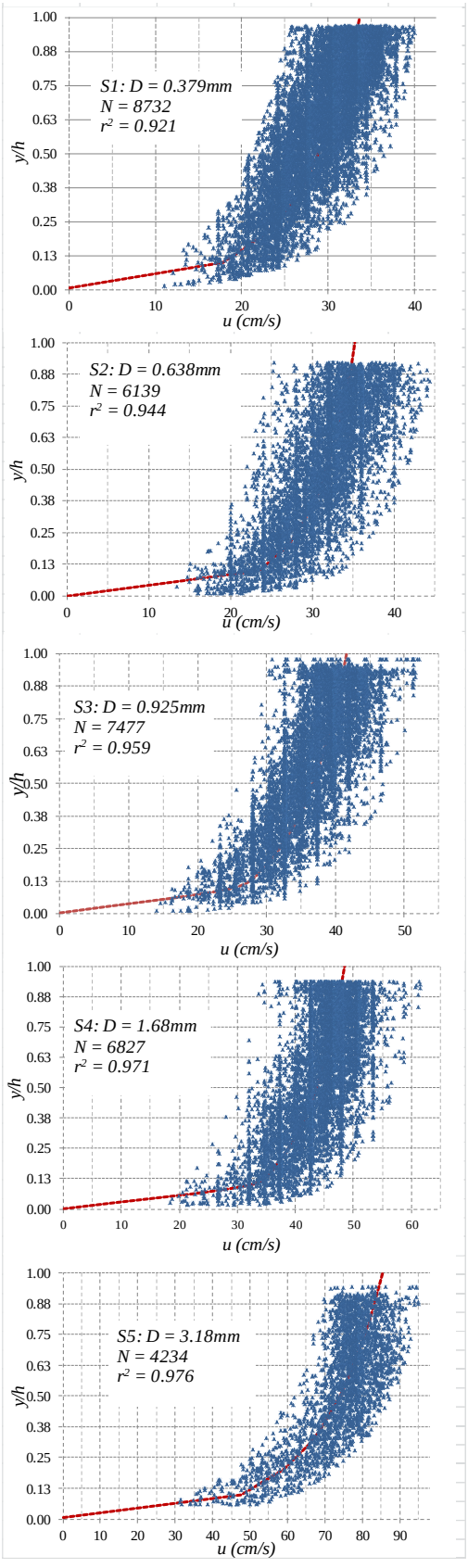

Fig. 3. Example of data from PTV and cross-correlation analysis.

Figure 4 shows the shields curve along with some of the results of this work. There is an agreement with Shields work even if Re* is calculated using D_{50}.

.

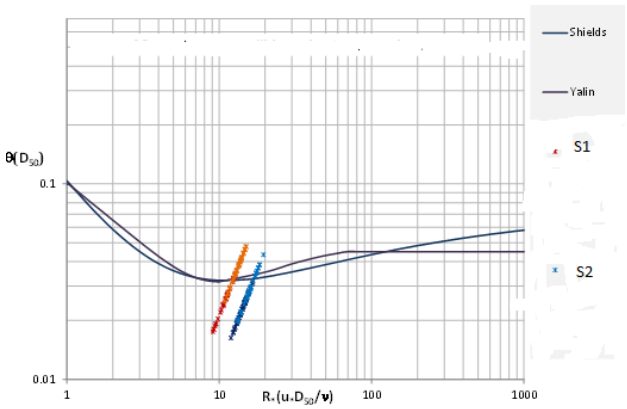

Fig. 4. $R_*(D_{50})$ vs Θ (for motion initiation); S1,S2.

The Reynolds stress distribution was calculated for each bed and is presented in the following figures

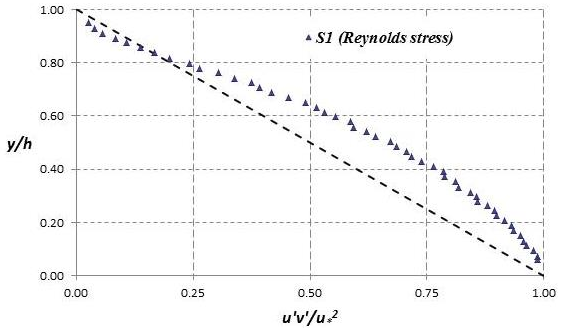

Figure 5. Reynolds stress distribution for sediment bed S1.

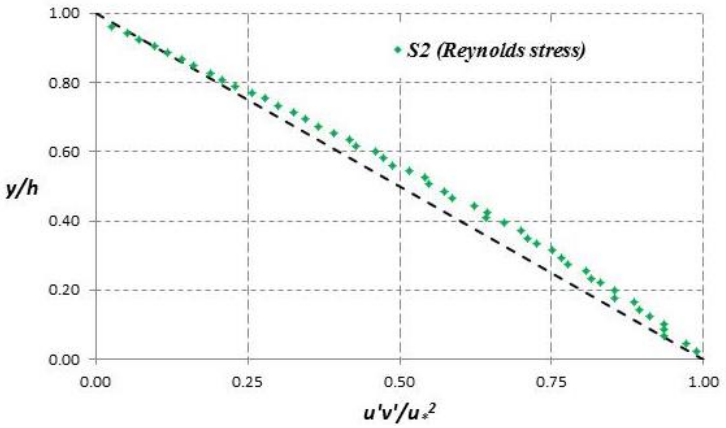

Fig. 6. Reynolds stress distribution for sediment bed S2

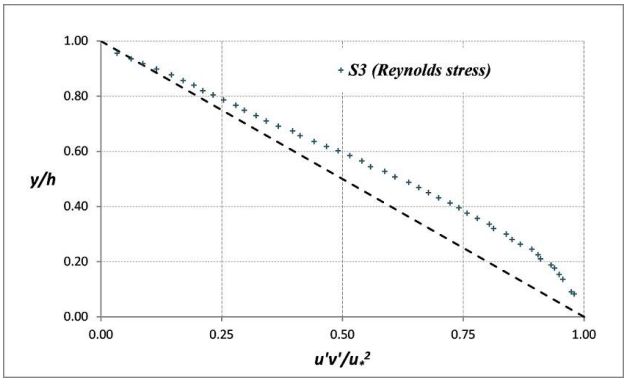

.

Fig. 7. Reynolds stress distribution for sediment bed S3

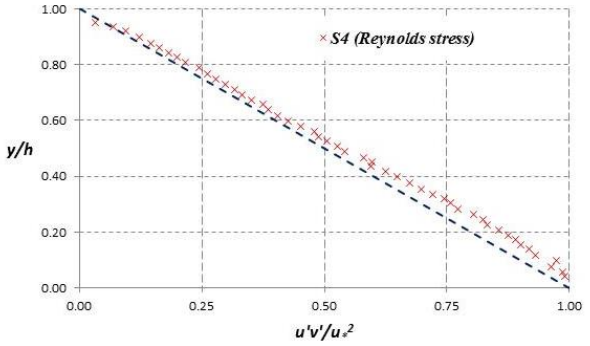

Fig. 8. Reynolds stress distribution for sediment bed S4

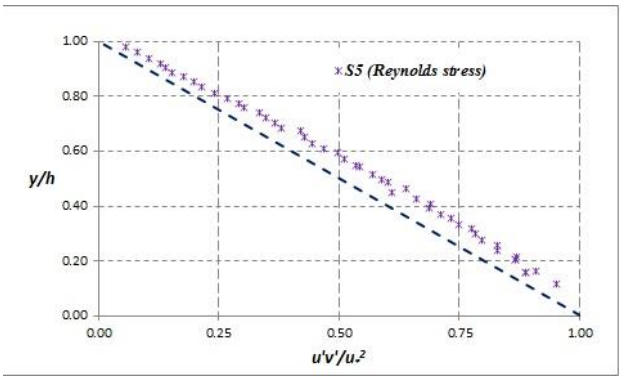

Fig. 9. Reynolds stress distribution for sediment bed S5

The values of Reynolds stress allowed us to calculate u_* and using equation 25 the values of k_s were obtained. Those values vary from 4.57 to 1.52 times D_{50} for the condition of motion initiation.. The mean rugosity k_s for each bed is presented in table 3. It is observed that bed rugosity is always larger than D_{50} and when D increases, k_s/D decreases

Table 3. Experimental bed rugosity k_s and relative rugosity k_s/D.

Loose bed	Average size $D_{50}(mm)$	Before and close motion	
		k_s (mm)	k_s/D_{50}
S1	0.379	1.733	4.573
S2	0.638	2.029	3.180
S3	0.925	2.909	3.144
S4	1.680	3.775	2.247
S5	3.180	4.847	1.524

Figure 10 shows the relationship between D and the relative rugosity *k*s /D. It can be observed that relative bed rugosity is larger for fine sand than for medium sand and fine gravel.

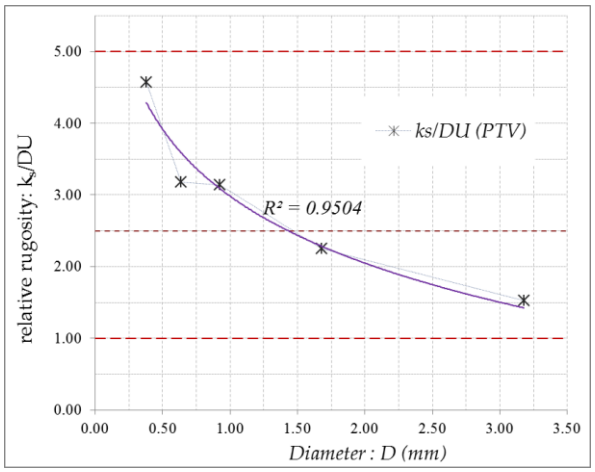

Fig. 10. Relationship between D_{50} and k_s/D_{50}

Critical mean velocities are similar to those obtained by Goncharov [21], Levy[22] , Chien and Wan [1] and Fuentes Carrasquel [16]. Table 4 shows this comparison where, in the case of Chien and Wan [1], the velocity is defined according to Einstein [20] graph and a bed rugosity $k_s = D_{65}$. In order to use Fuentes Carrasquel expression $k_s = D_{50}$ and the experimental critical shear stresses (table 2) . For Goncharov [21] and Levy [22], $k_s = D_{95}$ and $k_s = D_{90}$ respectively. PTV experimental results are also included

Table 4. Comparison of critical mean velocities

Loose bed	D (mm)	Critical mean velocity U_c (cm/s)				
		mean	theoretic			
		PTV	Goncharov $k_s = D_{95}$	Levy $k_s = D_{90}$	Chien – Einstein ks = D_{65}	Fuentes - Carrasquel
S1	0.379	25.809	23.929	31.591	28.084	33.581
S2	0.638	27.912	27.365	40.452	32.288	34.970
S3	0.925	31.848	32.899	47.340	36.782	37.428
S4	1.680	38.202	38.356	54.044	42.435	41.791
S5	3.180	no motion 70.252	45.599	64.542	50.325	49.669

As can be seen in table 4 almost all the formulas overestimate the experimental (PTV) mean critical velocity. Only for S5 bed, mean experimental

velocity is larger than theoretic. This is the one where no motion initiation was observed, but in this case the shear stress is less than the critical theoretic shear stress obtained by Shields or Yalin-Karahan criteria.

6- Conclusions

It has been shown experimentally, that for cohesionless sediments, accuracy of critical velocity profile depends on bed rugosity determination. It is a common practice in defining bed rugosity to use mean diameter or a constant representative diameter. In order to define bed rugosity for sands it should be taken into acount that relative bed rugosity for fine sand is larger than relative rugosity for medium sand and for fine gravel.

In order to apply as criteria for motion initiation the mean critical velocity, it should be used the apropiate bed rugosity that varies with the mean diameter D_{50}, according to figure 10. In this figure it is shown, the finding of this research, that relative bed rugosity decreases when the mean diameter D_{50} increases.

The experimental critical shear stresses obtained in this work, with the measured fluctuating velocities, are similar to those obtained by Shields curve.

It is recommended for future research to use more advanced optical techniques like Digital Holography in order to have more accuracy determining sediment motion initiation.

NOMENCLATURE

B = *constant in logarithmic velocity profile*

b_0, A = *constants in the regression*

D = *Mean particle diameter (mm)*

D_{35} = *Size larger than 35% (mm)*

D_{50} = *Size larger than 50% (mm)*

D_{65} = *Size larger than 65% (mm)*

D_{90} = *Size larger than 90% (mm)*

D_{95} = *Size larger than 95% (mm)*

D_{mn} = *Maximun size of particles(mm)*

D_{mx} = *Minimum size of particles (mm)*

d_{min}=*minimum distance for particle identification*

d_{max}=*maximum distance for particle identification*

g = *acceleration of gravity*

h = *Flow depth (cm)*

I= pixel intensity

k = *Von Karman constant = 0.4*

k_s = *Bed rugosity (mm)*

R = *Hydraulic radius (mm)*

R_* = *Reynolds of rugosity (-)*

Re_p = *Particle Reynolds (-)*

S = *Friction slope*

S1, S2, S3, S4, S5 = *Different sizes of sediment beds*

u = *Mean point velocity x-direction (cm/s)*

v = *Mean point velocity y-direction (cm/s)*

u_* = *Shear velocity (cm/s)*

$u´$ = *Fluctuating velocity u (cm/s)*

U_c = *Mean critical velocity (cm/s)*

U_x = *Mean flow velocity (cm/s)*

$v´$ = *Fluctuating velocity v (cm/s)*

V_m = *Mean velocity in vertical direction (cm/s)*

x_c,y_c= *coordinates of particle centroid*

y= *Distance from bed (cm)*

χ = *Einstein parameter (-)*

γ_s = *Specific weight of particles (N/m³)*

ν *Kinematic viscosity of water (m/s)*

θ *Shields parameter (-)*

ρ_s = *Particles density (kg/m³)*

τ_0 = *Bed shear stress*

τ_c = *Critical shear stress (N/m²)*

τ = *Reynolds stress (N/m²)*

7. References

[1] Chien N. and Wan Z. 1998. *Mechanics of Sediment Transport*; ASCE press, USA.

[2] Shields A. 1936. Anwendung der Aechlichkeitsmechanik und der turbulenzforschung auf die Geschiebewegung. *Mitt. Preussische Versuchsanstalt fur Wasserbau und Schiffbau*. Berlin, Germany.

[3] Yalin M.S. and Arahan E.K. 1979. Inception of sediment transport. *J. Hyd. Div. Proc. Amer. Soc. Civil Engrs*. Vol. 105. No. HY11, pp:1433-1443.

[4] Buffinton John M. 1999. The Legend of A. F. Shields. *Journal of Hydraulic Engineering.* Volume 125, Issue 4, pp. 376-387.

[5] Cao Zhixian; Pender Gareth and Meng Jian; 2006. Explicit Formulation of the Shields Diagram for Incipient motion of sediment. *Journal of Hydraulic Engineering*; Volume 132, Issue 10, pp. 1097-1099.

[7] García Flores Manuel, Maza Álvarez J. A. 1997. *Inicio de Movimiento y Acorazamiento*. Capitulo 8 Manual de Ingeniería de Ríos,UNAM-México.

[8] Ling Chi-Hai; 1995. Criteria for Incipient Motion of Spherical Sediment Particles. *Journal of Hydraulic Engineering*. Volume 121, Issue 6, pp. 472-478.

[9] Smith David A. 2004. Initiation of Motion of Calcareous Sand. *Journal of Hydraulic Engineering*. Volume 130, Issue 5, pp. 467-472

[10] Dancey Clinton L. Diplas P. Papanicolaou A. Bala Mahesh. 2002. Probability of individual grain movement and threshold condition. *Journal of Hydraulic Engineering*. Volume 128, Issue 12, pp. 1069-1075.

[11] Garde R. J; Sahay A. and Bhatnagar S. 2006. A simple mathematical model to predict the particle size distribution of the armour layer. *Journal of Hydraulic Engineering and Research*. Volume 38, Issue 5, pp. 815-821.

[12] Papanicolaou A.N. 2002. Stochastic Incipient Motion Criterion for Spheres under Various Bed Packing Conditions. *Journal of Hydraulic Engineering*; Volume 128, Issue 4, pp. 369-380.

[13] Hunziker Roni P. and Jaeggi Martin N. R. 2002. Grain sorting processes. *Journal of Hydraulic Engineering*. Volume 128, Issue 12, pp. 1060-1068.

[14] Kuhnle Roger A. 1993. Incipient Motion of Sand-Gravel Sediment Mixtures. *Journal of Hydraulic Engineering*. Volume 119, Issue 12, pp. 1401-1414.

[15] Sarmiento O. A. and Falcon M. A. 2006. Critical bed Shear Stress for unisize sediment. *Journal of Hydraulic Engineering*. Volume 132, Issue 2, pp. 172-179.

[16] Maza Álvarez J. A. García Flores M. 1984. *Hidrodinámica Bases para hidráulica fluvial*. Ed. Instituto de Ingeniería, UNAM-México.

[17] Salinas Tapia H. 2007. *Determinación de parámetros para flujo bifásico, sólido-líquido, aplicando técnicas ópticas.* Doctoral thesis. CIRA-Fac. Eng.-Universidad Autónoma del Estado de Mexico-México.

[18] Yang Shu-Qing, and McCorquodale John A. 2004; Determination of Boundary Shear and Reynolds Shear in Smooth Rectangular Channel Flows. *Journal of Hydraulic Engineering*. Volume 130, Issue 5, pp. 458-462.

[19] Lemmin Ulrich and Rolland Thierry. 1997. Acoustic Velocity Profiler for Laboratory and field Studies. *Journal of Hydraulic Engineering*. Volume 123, Issue 12, pp. 1089-1098.

[20] Einstein H.A. 1950. The bed load function of sediment transportation in open channel flows. US. Dept. Agri., technical bulletin 1026.

[21] Goncharov V.N. 1962. Basic river dynamics. *Hydro-Meteorological press*, Leningrad, Russia.

[22] Levy E.E. 1956. River Mechanics, *National Energy Press*, Moscow, Russia..

[23] Van Rijn L. 1982. Equivalent roughness of alluvial bed. *Journal of Hydraulic Engineering*. Volume 108, Issue 10, pp. 1215-1218.

[24] Smart Graeme M. 1999. Turbulent Velocity Profiles and Boundary Shear in Gravel bed Rivers. *Journal of Hydraulic Engineering*. Volume 125, Issue 3, pp. 106-116.

[25] Cheng Nian-Sheng and Chiew Yee-Meng. 1998. Modified logarithmic law for velocity distribution subjected to upward seepage. *Journal of Hydraulic Engineering*. Volume 124, Issue 12, pp. 1235-1241.

[26] Best Jim, Bennet Sean, Brige John and Leeder Mike. 1997. Turbulence modulation and particle velocities over flat sand beds at low transport rates. *Journal of Hydraulic Engineering*. Volume 123, Issue 12, pp. 1118-1130.

[27] Song T. and Graf W. H. 1996. Velocity and Turbulence Distribution in Unsteady Open Channel Flows. *Journal of Hydraulic Engineering*. Volume 122, Issue 3, pp. 141-196.

[28] Adrian Ronald J. 1991. Particle-Imaging techniques for experimental fluid mechanics. *Annual Review of Fluid Mechanics*. Volume 123; p.p. 43-6.

[29] Lazeroms W.M.J , Brethouwer G. , Wallin S. and Johansson A.V. 2013. An explicit algebraic Reynolds-stress and scalar-flux model for stably stratified flows. *Journal of Fluid Mechanics*. Volume 723,pp:91-125.

[30] Violeau, D. 2009 Explicit algebraic Reynolds stresses and scalar fluxes for density-stratified shear flows. *Phys. Fluids* 21, 035103